AS-TEXONO/01-03

June 29, 2001

Studies of Prototype CsI(Tl) Crystal Scintillators for Low-Energy Neutrino Experiments

Y. Liu[a], C.P. Chen[b], H.B. Li[b,c], C.H. Tang[c], C.Y. Chang[d], L. Hou[e], W.P. Lai[b,f], J. Li[a], S.T. Lin[b], C.S. Luo[b], J.F. Qiu[a], H.Y. Sheng[a,b], C.C. Wang[c], M.Z. Wang[c], S.C. Wang[b], H.T. Wong[b,1], B. Xin[e], Q. Yue[a], D.X. Zhao[a,b], S.Q. Zhao[a,g], Z.Y. Zhou[e], B.A. Zhuang[a,b]

The TEXONO[2] Collaboration

[a] Institute of High Energy Physics, Beijing, China.

[b] Institute of Physics, Academia Sinica, Taipei, Taiwan.

[c] Department of Physics, National Taiwan University, Taipei, Taiwan.

[d] Department of Physics, University of Maryland, College Park, U.S.A.

[e] Department of Nuclear Physics, Institute of Atomic Energy, Beijing, China.

[f] Department of Management Information Systems, Chung Kuo Institute of Technology, Taipei, Taiwan.

[g] Unique New Materials Company, Beijing, China.

[1]Corresponding author: Email: htwong@phys.sinica.edu.tw; Tel:+886-2-2789-9682; FAX:+886-2-2788-9828.

[2]Taiwan EXperiment On NeutrinO

Abstract

Crystal scintillators provide potential merits for the pursuit of low-energy low-background experiments. A CsI(Tl) scintillating crystal detector is being constructed to study low-energy neutrino physics at a nuclear reactor, while projects are underway to adopt this technique for dark matter searches. The choice of the geometrical parameters of the crystal modules, as well as the optimization of the read-out scheme, are the results of an R&D program. Crystals with 40 cm in length were developed. The detector requirements and the achieved performance of the prototypes are presented. Future prospects for this technique are discussed.

PACS Codes: 14.60.Lm, 29.40.Mc.

Keywords: Neutrinos, Scintillation detectors.

Submitted to Nucl. Instrum. Methods. **A**

1 Introduction

Crystal scintillators have been widely used as radiation detectors and in medical imaging [1]. Large detector systems, of scale several tens of tons in mass, have been constructed and made operational for high energy physics experiments [2].

The merits of this detector technology in non-accelerator particle physics experiments have been recently discussed [3]. Primarily, the high-Z composition of most crystals allows a compact design and provides large suppression of background due to ambient radioactivity if a three dimensional fiducial volume definition can be realized. An experiment based on 100 kg of NaI(Tl) has been built for Dark Matter searches, producing some of the most sensitive results [4].

This article reports on the results of an R&D program on CsI(Tl) crystal scintillator [5] performed by the TEXONO Collaboration towards a 500 kg CsI(Tl) detector system to be installed close to a nuclear reactor core of the Kuo-Sheng (KS) Power Plant in Taiwan to study low energy neutrino interactions [6, 7]. Scintillating CsI(Tl) crystals [8] have the merits of providing large light yield, low energy threshold and with pulse shape discrimination characteristics for γ/α separation. Its property of being only slightly hygroscopic implies that it can be machined easily and does not require hermetic seal (that is, passive materials) in a large detector system. In addition, large (40 tons) electromagnetic calorimeter systems [9] have been constructed and made operational in high energy physics experiments, making this technology affordable and realistic to scale up. Considering all the associated costs, the price of CsI(Tl) is in fact less than that for NaI(Tl).

To achieve a three-dimensional fiducial volume definition with minimal passive materials and dead space, the detector modules are hexagonal in shape and stacked together as depicted in Figure 1. The system is placed in a dry nitrogen atmosphere to minimize humidity and to purge the radioactive radon gas. The scintillation light is read out by photo-multipliers (PMTs) at both ends of the modules. The sum of the signals gives the energy of the event while their difference provides information of the longitudinal position. The PMT signals are shaped and amplified and subsequently digitized by a 20 MHz Flash Analog to Digital Convertor (FADC) system [10]. Timing-correlation of possible delayed-cascade events are also recorded for the purposes of background identification and rejection.

The background from ambient radioactivity or intrinsic radio-purity are of course crucial to all low-background experiments. Their considerations for CsI(Tl) detectors are discussed in Refs. [3, 7, 11]. Levels of better than the 10^{-12} g/g level in concentration for the ^{238}U and ^{232}Th series have been demonstrated, assuming secular equilibrium. With the detector hardware giving satisfactory performance, the background issues will be the principal focus with the actual data taking on-site and their control with determine the sensitivities of the experiment.

The following sections discuss the choice of parameters leading to the present detector design as well as the performance of the different options in the prototype studies.

2 Scintillating CsI(Tl) Crystal

2.1 Fabrication

The CsI(Tl) crystals are produced by the Bridgman-Stockbarger method [12] in a quartz crucible [13] 10 cm in diameter and 50 cm in length[3]. The raw materials include CsI powder[4] and 1500 ppm of the dopant thallium iodine (TlI) powder, both purified by baking in vacuum. The crystal growth was also performed in vacuum. The oven temperature is maintained at 500^{o}C to 800^{o}C along the crystal growing axis with the melting point of 621^{o}C at the growing interface. The growth rate is about 1 mm per hour.

The Tl concentration at the 400 ppm to 2000 ppm range can provide a reasonable scintillation yield. The examination on the uniformity of the light output along the longitudinal axis is therefore necessary to ensure the quality of the crystal. This requirement of uniform Tl concentration places constraint upon the length of crystal growth. Variation of Tl concentration results in difference in light yield as well as changes in the rise and

[3]Producer: Unique Crystal, Beijing

[4]Supplier: Chemetall, GmBH, Germany

decay times of heavily ionizing events like α-particles and nuclear recoil. Timing response to γ-events is unaffected [8].

Crystal modules produced for the Kuo-Sheng experiment are of two categories: Batch I consists of two pieces of 20 cm crystals glued together to form a 40 cm module ("L20+20"); Batch II are CsI(Tl) single crystal of 40 cm in length ("L40"). The actual growth length is 50 cm from which 40 cm is cut out and turned into an active detector. This is the longest single crystal of CsI(Tl) reported for industrial production. The hot forging method which can be used to produce large-volume multi-crystalline NaI(Tl) detector [14] is not applicable to produce large CsI(Tl) multi-crystals. Cracks readily develop along the crystal interfaces upon mechanical stresses.

Both the L20+20 and L40 detector modules are hexagonal in shape of size 2 cm, giving a cross-section area of 10.4 cm^2, and a mass of 1.88 kg per module. They can be stacked up into a big fiducial volume with minimal dead space and passive materials. The goal of the prototype measurements is to optimize the crystal parameters to achieve good energy and longitudinal position resolutions.

2.2 Crystal Characteristics

The main characteristic properties of CsI(Tl) scintillating crystals [8], together with a few other common scintillators, are listed in Table 1.

Undoped CsI emits at ultra-violet (peaks at 310 nm), has very fast decay time (10 ns), and is radiation hard [8, 15]. Effects of an admixture of Tl are to absorb the UV emissions, and shift the spectra to green, via the Tl^+ luminescence [16]. The emission peaks at about 530-560 nm, as confirmed by the measured emission spectrum by a fluorescence spectrophotometer[5], as displayed in Figure 2. Overlaid on top are typical response due to photo-multiplier tube (PMT) with bi-alkaline photo-cathode and silicon photo-diode (PD).

In principle, CsI(Tl) would produce about 50000 photons per MeV of electron-equivalence

[5]Hitachi F-3010

energy deposition, similar to the range of that for NaI(Tl). However, since the spectral response of typical PMTs with bi-alkaline photo-cathode do not match well to the emission spectrum, the effective photo-electron yield is typically only half of that of NaI(Tl).

2.3 Pulse Shape Discrimination

The light emissions of CsI(Tl) exhibit different shape for electrons (that is, minimum ionizing particles) α-particles and nuclear recoils, as depicted in the FADC measurement in Figure 3a. It can be seen that heavily ionizing events due to α-particles and nuclear recoils have *faster* decays than those from γ's – opposite to the response in liquid scintillator [16]. This is the basis of the particle identification of this scintillator [17].

Fitted to an analytical form of the pulse shape(y) as a function of time(t)

$$y \ = \mathrm{Constant} * [\ 1 - \exp(-\frac{t}{\tau_0})\ ] * [\ \frac{1}{\tau_1}\ \exp(-\frac{t}{\tau_1}) + \frac{r}{\tau_2}\ \exp(-\frac{t}{\tau_2})\ ] \tag{1}$$

for the light profile from γ/α events, one obtains the fitted-values of rise time(τ_0) and fall times(τ_1, τ_2) as well as the ratio between the slow and fast decay components(r) as tabulated in Table 2. The values of τ_0 in CsI(Tl) are dominated by the electronics shaping rise time of 250 ns for > μs pulses [10]. The intrinsic rise times of the CsI(Tl) scintillator are expected to ∼125 ns and ∼20 ns for γ- and α-events, respectively [8].

The difference in the decay time constants between γ and the ions (α and nuclear recoils) forms the basis of pulse shape discrimination (PSD). A well-established way to achieve PSD is by the "double charge method" [18]. By comparing the "total charge" (Q_t: integration over 4 μs) and the "partial charge" (Q_p: integration for the same duration *after* a delay of 0.5 μs), discrimination of γ/α can be achieved with >99% efficiency down to about 100 keV electron-equivalence light output, as shown in Figure 4. The difference in pulse shape for nuclear recoils provides a potential advantage to adopt the CsI(Tl) crystal for Dark Matter searches [19].

Unlike in liquid scintillators, α's are only slightly quenched in their light output in CsI(Tl) [16]. The quenching factor depends on the Tl concentration and the α-energy [8]. For full integration of the signals, the suppression is typically 50% at the α-energy of

5.4 MeV for a ^{241}Am source, as compared to a typical quenching factor of 10 in liquid scintillator. This small quenching as well as a distinguishable α-signature make this crystal a very good detector for measuring α and heavy-ions events in, for instance, the tagging of events due to internal radioactivity from the ^{238}U and ^{232}Th cascades.

The quenching factors for the recoils of Cs and I ions are larger, and are typically at the range of 10−20% at recoil energy less than 50 keV [19, 20], the energy range relevant for Dark Matter experiments.

2.4 Temperature Effects

It is well-established that crystals like CsI(Tl) and NaI(Tl) give higher light yield with increasing temperature at typical laboratory conditions (room temperature). As depicted in Figure 5, measurements were made to confirm this with our crystals, giving a enhancement coefficient of $(5.8 \pm 0.5) \times 10^{-3}\ ^{o}C^{-1}$.

However, the typical drop in PMT efficiencies (a typical value is $-3 \times 10^{-3}\ ^{o}C^{-1}$ at 525 nm) as well as the increase of electronic noise in PD readout with rising temperature tend to offset this advantage of higher light yield. Indeed, at the large photo-electrons regime for PD readout (where performance is limited by electronic noise), a 10% better energy resolution was observed by operating around 5^{o}C where the light yield drops by 10%.

The results reported in the following sections are based on measurements done at "room" temperature of about 20^{o}C.

3 Prototype Detectors

3.1 Crystal Geometry

To achieve a three-dimensional fiducial volume definition with minimal passive materials and dead space, the detector modules are hexagonal ("honey-comb") in shape and stacked together as in Figure 1. The crystals are either the L20+20 or the L40 type. The length of 40 cm is long compared to the hexagon cross-section whose sides are 2 cm. This is to provide a variation of light collection to establish a longitudinal distance measurement.

The surfaces are cut and polished with aluminium oxide powder to the "reflection" (/R) or "scattering" (/S) grade – the former refers to a surface flatness of better than 0.5 μm which allows total internal reflection, while the latter has a flatness of 3 μm such that light is propagated by "diffused" scatterings. The selection between these surfaces is based on the optimization between energy resolution, which requires maximum light collection and position resolution, which requires a certain level of attenuation effects along the length of the crystal.

To maximize the light collection, the crystals are wrapped with four layers of 70 μm thick teflon sheets whose purposes are to provide another diffused scattering surfaces to capture the escaped photons back to the crystal, and to prevent the cross-talks among adjacent crystal modules. The results to the cross-talk studies are displayed in Figure 6 where a LED pulse is illuminated on to a PMT through a varying number teflon sheets. It can be seen that the light intensity is attenuated by 90% by a single layer. Starting from the third layers, the attenuation factor is about 0.5 per layer. These effects can be explained by multiple-bouncing of the scattered light within multiple teflon layers. The total attenuation after traversing eight layers (boundary of two adjacent modules) is 4×10^{-4}, ensuring that cross-talks are minimal even for high energy events up to 10 MeV.

In this intensity setting, the single photo-electron level was reached after 8 layers where the ADC-peak positions were not reduced further and only that the fraction of the "pedestal" (sampling of zeros) events increased. This gives a convenient way to monitor single photo-electron responses of PMTs.

By comparing the photo-peaks of events due to a ^{137}Cs γ-source for a L20+20 crystal, the teflon wrappings enhance light collection by 50% relative to the one with no wrappings and collects light only by total internal reflection from the bare crystal surface.

3.2 Readout Device

In principle, the silicon PIN photo-diode (PD) gives better quantum efficiency and matching in the spectral response for CsI(Tl) crystals than the PMTs with bi-alkali photocathode, as indicated in Figure 2. Indeed, calorimeters in high energy collider experiments (where the events are of GeV range) typically adopt PD readout for its compactness and its being insensitive to magnetic field.

However, the PDs have smaller light collection area and require pre-amplifiers (PA) for readout. The threshold and energy resolution is dominated by electronic noise which depends on the dark current and input capacitance of the PDs. Using the 60 keV γ-ray from ^{241}Am as a calibration, one can establish the combined electronic noise of a 2 cm$\times$1 cm PD[6] plus PA[7] is 580 photo-electrons.

For low energy experiment on keV-range events, the PMTs gives superior performance in terms of resolution and threshold due to their low noise level of a few photo-electrons, An illustration of their different performance can be found in Figure 7, where the measured energy spectra for ^{137}Cs by both devices on a 2.54 cm diameter and 2.54 cm length CsI(Tl) crystal are shown. The FWHM resolution at 660 keV are 14.3% and 8.4%, respectively, for PD and PMT. The electronic noise threshold also improves from $\sim$100 keV to $\sim$10 keV from PD to PMT.

Accordingly, a 29 mm diameter PMT[8] with low-activity glass window and envelope was chosen for the experiment. A dynamic range with linear response of better than a factor of 1000 is achieved after optimizations of PMT-base circuit design. The results reported in subsequent sections are based on this PMT coupled to the crystal surface via optical grease.

[6] Hamamatsu S2744-08

[7] Canberra 2006

[8] Hamamatsu CR110 customized

3.3 Prototype Performance

The performance of prototype modules (L20+20/S, L40/R, L40/S with definitions as described in Section 2.1) can be derived from the measurement with radioactive sources of different energy.

As discussed in Ref. [10], the PMT signals are fed into a Amplifier+Shaper module, the output of which are recorded by a 20 MHz, 8-bit Flash Analog Digital Convertor (FADC) on a VME-bus. A typical signal due to a ^{137}Cs source as measured by the CsI(Tl)+PMT with a 100 MHz digital oscilloscope is displayed in Figure 8a. The pulse after electronics shaping and recorded by the FADC is shown in Figure 8b.

The sum of the two PMT signals from the two ends ($Q_{tot} = Q_1 + Q_2$) gives the energy of the event. The longitudinal position can be derived by the variation of the dimensionless ratio $R = (Q_1 - Q_2)/(Q_1 + Q_2)$ with position.

The values of Q_{tot} depends on integration time defined by software, the optimal range of which are different for different energies. The FWHM resolution of 660 keV from ^{137}Cs and 30 keV from ^{133}Ba as function of integration time are shown in Figure 9 to illustrate this effect. Typical spectra of Q_1, Q_2 and Q_{tot} due to a ^{133}Ba source for the L40/R crystal are displayed in Figure 10. It can be seen that a threshold level of $\sim$10 keV are readily achievable. The calibration for Q_{tot} is about 1 keV per photoelectron, as derived from the PMT single photo-electron response with an attenuated LED source, as discussed in Section 3.1.

3.3.1 The L20+20/S Crystal

The L20+20/S module are constructed from two pieces of 20 cm CsI(Tl) crystals glued together. Each piece has a light yield uniformity of better than 5% along the 20 cm length, based on measurements with a PMT coupled to one side with the other end also covered by teflon sheets.

The variation of light collection across the length of the crystal for Q_1, Q_2 and Q_{tot} are displayed in Figures 11a. The charge unit is normalized to unity at the ^{137}Cs photo-peak

(660 keV) for both Q_1 and Q_2 at their respective ends, while the error bars denote the FWHM width at that energy. A FWHM resolution of 10% is achieved.

The discontinuity at L=20 cm is due to the optical mis-match between the glue (n=1.5) and the CsI(Tl) crystal (n=1.8). Typically, there is a 20% drop in the light collection across the glued boundary. It can be seen that there is a dependence of Q_{tot} with position at the 10-20% level.

Readout with PMTs at both ends would produce a larger non-uniformity in total light collection with position, as compared to light collection only at one end with the other end covered with teflon sheets. The teflon serves as a reflecting surface to bounce back the light which would otherwise leak out in the case of the two-end readout configuration.

The longitudinal position can be obtained by considering the R-value, where its variations at the ^{137}Cs photo-peak energy along the crystal length is displayed in Figure 11b. The ratio of the RMS errors in R relative to the slope gives the longitudinal position resolution of better than 2 cm RMS at 660 keV.

3.3.2 The L40 Crystal

The L40 crystals are single crystals of CsI(Tl) with 40 cm in length. These were developed and turned into large-scale production during the course of our R&D program. Light yield uniformity is better than 8%, while the decay time profiles are constant to better than 4%. In the prototype measurements, crystals with both reflection (/R) and scattering (/S) grades surfaces were studied.

The light collection and R-value variations across the length for the L40/R and L40/S crystals with a ^{137}Cs γ-source are shown in Figures 12a and 12b, respectively. It can be seen that the light transmission of the /S-grade is slightly worse than the /R-grade, as indicated by an "effective attenuation length" of 24 cm versus 30 cm, respectively. The FWHM energy resolutions are 11% for both at the central position. The larger slope in R for the /S-grade crystal is offset by bigger uncertainties, such that the RMS longitudinal position resolutions are $\sim$2 cm in both cases.

Therefore, the L40 crystals give similar performance to the L20+20 crystals but without the discontinuity which complicates the subsequent event re-construction. The /R and /S grades do not give rise to big difference in performance.

The variations of the energy resolution with energy for both crystal types are shown in Figures 13a. A FWHM energy resolution of 10% is achieved at 660 keV. The variations of longitudinal position resolution with energy are depicted in Figure 13b. The measured RMS-resolutions are 3.8 cm and 6.7 cm at 80 keV and 30 keV, respectively. Only upper limits of 2 cm can be derived above 350 keV, since the interaction points are no longer localized due to finite collimator width as well as the dominant multiple Compton scatterings at these higher energy. There is no energy dependence of the slopes R to better than 5%. The linearity of the energy response is illustrated in Figure 13c, providing a convenient calibration using standard γ-sources.

3.3.3 Light Guide with Undoped-CsI

As indicated in Figure 13b, a longitudinal position information (or fiducial volume cut) can be derived for energies above 300 keV. For low energies such as that at the 10 keV range relevant for Dark Matter experiments, the RMS resolution is big such that the fiducial volume definition becomes inefficient.

An approach to achieve a three-dimensional volume definition at low energies is to use active light guide at both ends. The entire fiducial volume are enclosed by a high-Z, high-density active veto volume, suppressing external background. The light guide materials should have a different decay curve from the target crystal such that events originating at the light guide can be easily identified by pulse shape discrimination.

The undoped-CsI crystal [15] is optimal for this purpose, having fast decay time ($\sim$10 ns) as compared to CsI(Tl) ($\sim$1000 ns) as depicted by the measured light curves in Figure 3b. The fitted values of τ_0 and τ_1 listed in Table 2 only reflect the electronics shaping time of 27 ns for fast ($\sim$10 ns) pulses as well as the finite time bin (50 ns) for the FADC. The emission spectrum of pure CsI peaks at the ultra-violet range and the relative photo-electron yield is only about 0.1 of that for CsI(Tl) with a bi-alkaline PMT.

Measurements were carried out with the L40/R crystal with undoped-CsI light guides optically coupled at both ends (L40/R+LG). The light guides have the same hexagonal cross-section area and are 3 cm in length. The comparisons of light collection and of the R-values are displayed in Figures 14a and 14b, respectively. It can be seen that the L40/R+LG module gives similar performance in terms of energy and longitudinal position resolutions, as compared to the L40/R crystal.

The light collection is inevitably reduced with the addition of light guides. It is, however, interesting to note that the reduction factor is larger ($\sim$10%) at the near end. Only a marginal effect is observed at the far end. This can be explained by the fact that light propagation is more forward (that is, less back-scattering due to total internal reflection at the crystal-glue interface) for events taking place at the far ends.

The fiducial CsI(Tl) target is totally protected from ambient radioactivity in a detector configuration shown in Figure 1 but with active light guide at both ends. The suppression is especially strong at low energies. For instance, the attenuation length of an 100 keV γ-ray in CsI is 0.12 cm, such that it is essentially impossible for external γ-background at this energy to penetrate the 3 cm light guides.

4 Summary and Prospects

The research program of the TEXONO Collaboration evolves around the theme of exploring the use of crystal scintillators for low-energy low-background experiments for neutrino and astro-particle physics [3, 6].

An extensive R&D program was carried out to investigate the use of CsI(Tl) scintillating crystals. We report on the results of the prototype studies in this article. The major detector requirements and challenges are the simultaneous optimization of low threshold, large dynamic range, good energy resolution, position resolution and pulse shape discrimination.

Long single crystals of 40 cm length were successfully developed and turned into production mode during the course of the R&D program. The performance are similar among the L20+20 and L40 modules, and so between /S- and /R-grades surface treatment. The addition of undoped-CsI light guides do not give notice-able degradation. The results displayed in Figure 13 indicate the capabilities for all these cases, which have the same modular mass of about 2 kg. The typical ranges are 10% for the FWHM energy resolution at 660 keV, better than 2 cm RMS position resolution at energy above 400 keV, 10 keV energy threshold, and better than 99% PSD capabilities above 100 keV electron-equivalence energy. In contrast, the performance can deteriorate dramatically if photo-diode readout is used or if the teflon wrapping sheets are not applied.

For the Kuo-Sheng Reactor Neutrino Experiment [7], a total of 100 kg of the L20+20/S crystals were produced before the L40 crystals were developed. Subsequent production will focus on the L40/R crystals. As discussed, both configurations give similar performance nominally, but the event reconstruction algorithms will be simpler for the L40 crystals. The options were kept for using undoped-CsI as light guide for future upgrades. Data taking starts in 2001 with 100 kg of crystal modules.

A good longitudinal position resolution, and hence a three-dimensional fiducial volume definition, is possible for energy above 300 keV under the present geometry. For lower energies, undoped-CsI as active veto and light guide can be used to provide this desirable feature.

The measurements under different configurations reported here can be used to develop simulation software to study the characteristic parameters for light transmission, reflection and scattering in CsI(Tl) crystals [21]. Such tools would be valuable in the future design of experiments requiring other detector geometries.

This work demonstrates that the production of CsI(Tl) scintillating crystals with length up to 50 cm is possible. In addition, different crystals can be glued together forming larger modules while maintaining the good mechanical strength and optical transmission. Therefore, it is possible to have detectors with individual modules ~1 meter in length. Lateral dimension depends on the size of the crucible and the range of 15 cm is realistic. To maintain similar or better light transmission and collection, the "length-to-diameter" ratio of the detector module should be comparable or more than 10 (40 cm:4 cm in the present case). As an illustration, a $15 \times 15 \times 100$ cm^3 CsI(Tl) crystal would give a modular mass of about 100 kg, such that a 50 ton detector can be integrated from only 500 channels. It is also possible to have a "phoswich" detector composed of different scintillator crystal modules and/or light guides glued together. The event locations can be identified by pulse shape discrimination techniques.

The use of CsI(Tl) crystals for Dark Matter searches were recently discussed [19]. The main detector requirements would be to minimize the threshold and to perform PSD for γ's and nuclear recoil events at very low electron-equivalence (typically few keV) energy [21]. Results reported in this article are relevant to adapt this crystal for Dark Matter experiments. Light guides will be essential at this low energy range to define an inner fiducial volume.

Low energy solar neutrino experiment is another exciting area where scintillating crystals may have potential advantages, being one of the few technologies where a wide range of nuclei can be incorporated into an active detector. Crystals with indium [22] and lithium [23] have been investigated, while there are much interest recently on gadolinium and ytterbium based crystals [24, 25]. The challenge is to be sensitive to the signal rate of the range of 1 event per day per 10 tons of target materials such that the requirements of intrinsic radio-purity are extremely stringent. While the crystals may be different, the essential design concept of the KS reactor experiment to achieve a three-dimensional fiducial volume definition are applicable.

The authors are grateful to the technical staff of our institutes for invaluable support. This work was supported by contracts NSC 88-2112-M-001-007, NSC 89-2112-M-001-028 and NSC 89-2112-M-001-056 from the National Science Council, Taiwan, 19975050 from the National Science Foundation, China, as well as CosPa 89-N-FA01-1-4-2 from the Ministry of Education, Taiwan.

References

[1] For a recent review on the crystal scintillator detector, see, for example, M. Ishii and M. Kobayashi, Prog. Crystal Growth and Charact., **23**, 245 (1991), and references therein.

[2] For a recent review on the applications of crystal scintillator in particle physics, see, for example
G. Gratta, H. Newman, and R.Y. Zhu, Ann. Rev. Nucl. Part. Sci. **44**, 453 (1994).

[3] H.T. Wong et al., hep-ex/9910002, Astropart. Phys. **14**, 141 (2000).

[4] R. Bernabei et al., Phys. Lett. **B 389**, 757 (1996);
R. Bernabei et al., Phys. Lett. **B 450**, 448 (1999).

[5] Yan Liu, Ph.D. Thesis, Institute of High Energy Physics, Beijing, China (2000).

[6] H.T. Wong and J. Li, Mod. Phys. Lett. **A 15**, 2011 (2000).

[7] H.B. Li et al., TEXONO Collaboration, hep-ex/0001001, Nucl. Instrum. Methods **A 459**, 93 (2001).

[8] H. Grassmann, E. Lorentz and H.G. Moser, Nucl. Instrum. Methods **228**, 323 (1985);
P. Schotanus, R. Kamermans, and P. Dorenbos, IEEE Trans. Nucl. Sci. **37**, 177 (1990).

[9] Y. Kubota et al., CLEO Coll., Nucl. Instrum. Methods **A 320**, 66 (1992);
E. Aker et al., Crystal Barrel Coll., Nucl. Instrum. Methods **A 321**, 69 (1992);
Letter of Intent, Belle Coll., KEK (1993);
Letter of Intent, BaBar Coll., SLAC-443 (1994).

[10] W.P. Lai et al., TEXONO Collaboration, hep-ex/0010021, Nucl. Instrum. Methods **A 465**, 550 (2001).

[11] U. Kilgus, R. Kotthaus, and E. Lange, Nucl. Instrum. Methods **A 297**, 425, (1990);
R. Kotthaus, Nucl. Instrum. Methods **A 329**, 433 (1993).

[12] P.W. Bridgman, Proc. Amer. Acad. Arts Sci. **60**, 306 (1925);
D.C. Stockbarger, Rev. Sci. Instrum. **7**, 133 (1936)

[13] I.M.S. Sidawi and S.N. Tewari, J. Crystal Growth **131**, 230 (1993).

[14] O.H. Nestor, in *Proc. of Mat. Res. Soc. Symp.*, Nuclear Radiation Detector Materials **16** 77 (1983).

[15] S. Kubota et al., Nucl. Instrum. Methods **A 268**, 275 (1988).

[16] See, for example, "Theory and Practice of Scintillation Counting", J.B. Birks, Pergamon (1964).

[17] J. Alarja et al., Nucl. Instrum. Methods **A 242**, 352 (1982);
F. Benrachi et al., Nucl. Instrum. Methods **A 281**, 137 (1989).

[18] C.L. Morris et. al., Nucl. Instrum. Methods **137**, 397 (1976);
M.S. Zucker and N. Tsoupas, Nucl. Instrum. Methods **A 299**, 281 (1990).

[19] S. Pecourt et al., Astropart. Phys. **11**, 457 (1999);
E. Won et al., Nucl. Phys. **B** (Procs. Supp.) **78**, 449 (1999);
V.A. Kudryavtsev et al., Nucl. Instrum. Methods **A 456**, 272 (2001).

[20] M.Z. Wang et al., in preparation for Phys. Rev. **C** (2001).

[21] C.H. Tang et al., in preparation for Nucl. Instrum. Methods **A** (2001).

[22] R.S. Raghavan, Phys. Rev. Lett. **37**, 259 (1976);
L. Gonzalez-Mestres and D. Perret-Gallix, Nucl. Instrum. Methods **A 279**, 382 (1989);
J.P. Chaminade et al., J. Cryst. Growth **99**, 799 (1990);
M. Avenier et al., Nucl. Phys. **B** (Proc. Suppl.) **28A**, 496 (1992).

[23] C.C. Chang, C.Y. Chang, and G. Collins, Nucl. Phys. (Proc. Suppl.) **B 35**, 464 (1994).

[24] R.S. Raghavan, Phys. Rev. Lett. **78**, 3618 (1997).

[25] S.C. Wang, H.T. Wong, and M. Fujiwara, hep-ex/0009014, Nucl. Instrum. Methods **A**, in press (2001).

Properties	CsI(Tl)*	CsI(pure)	NaI(Tl)	BGO	Liquid	Plastic
Density (gcm^{-3})	4.51	4.51	3.67	7.13	0.9	1.0
Relative Yield [II]	0.45	0.05	1.00 †	0.15	0.4	0.35
Radiation Length (cm)	1.85	1.85	2.59	1.12	∼45	∼45
dE/dx for MIP ($MeVcm^{-1}$)	5.6	5.6	4.8	9.2	1.8	1.9
Emission Peak (nm)	565	310	410	480	425	425
Decay Time (ns)	1000	8	230	300	2	2
Refractive index	1.79	1.95	1.85	2.15	1.5	1.6
Hygroscopic	slightly	slightly	yes	no	no	no

* At 1500 ppm dopant concentration

[II] Effective photo-electron yield from bi-alkaline photo-cathode.

† Typical light yield for NaI(Tl) is about 40000 photons per MeV.

Table 1: Characteristic properties of the common crystal scintillators and their comparison with typical liquid and plastic scintillators.

Crystal	Event Type	Rise Time [τ_0 (ns)]	Decay Time Constant		Ratio (r)
			Fast Comp. [τ_1 (μs)]	Slow Comp. [τ_2 (μs)]	
CsI(Tl)	α	203±3	0.54±0.1	2.02±0.02	0.29±0.02
CsI(Tl)	γ	261±2	0.87±0.1	5.200.04	0.61±0.01
CsI(pure)	γ	∼0.55	0.19±0.01	–	–

Table 2: Fitted rise and decay time constants as well as the ratio between slow and fast decay components for α and γ events measured by CsI(Tl) and undoped CsI.

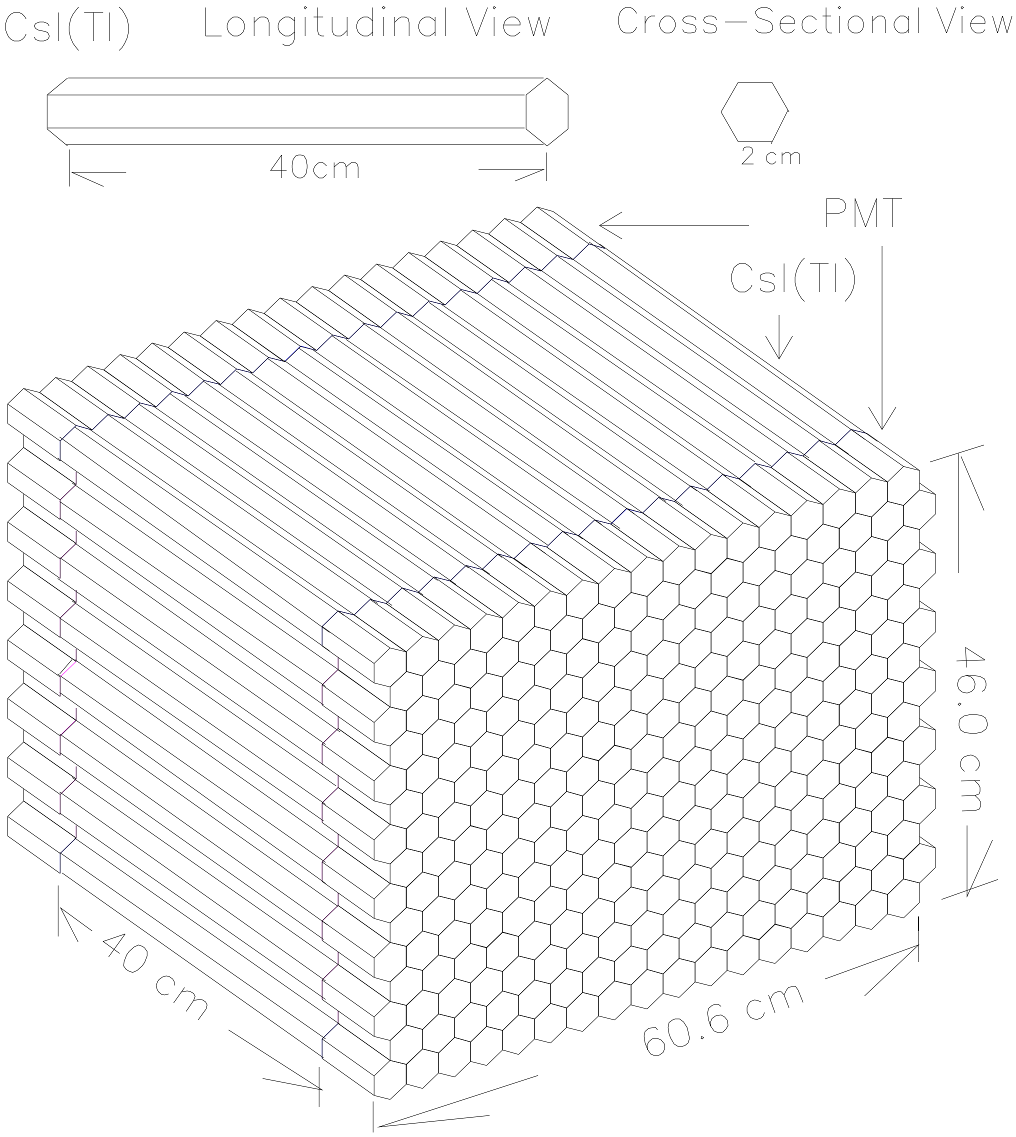

Figure 1: Schematic drawings of the CsI(Tl) detector under construction for the Kuo-Sheng experiment, showing a 2(Width)$\times$17(Depth)$\times$15(Height) matrix. Individual crystal module is 40 cm long with a hexagonal cross-section of 2 cm edge. Readout is performed by photo-multipliers at both ends.

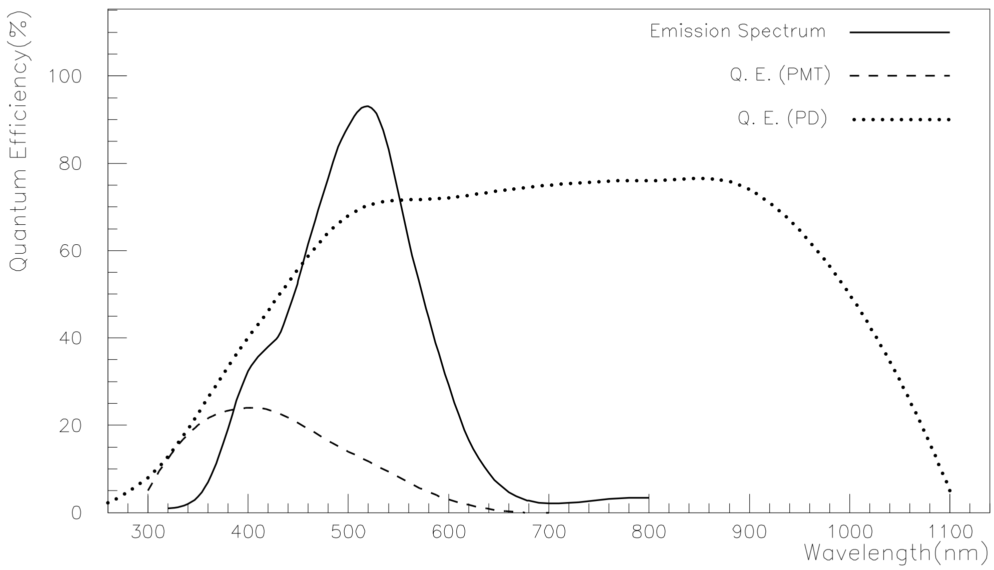

Figure 2: Measured emission spectra, in arbitrary units, from a CsI(Tl) crystal. The typical quantum efficiencies from a photo-multiplier with bi-alkaline photocathode and from a silicon photodiode are overlaid.

(a)

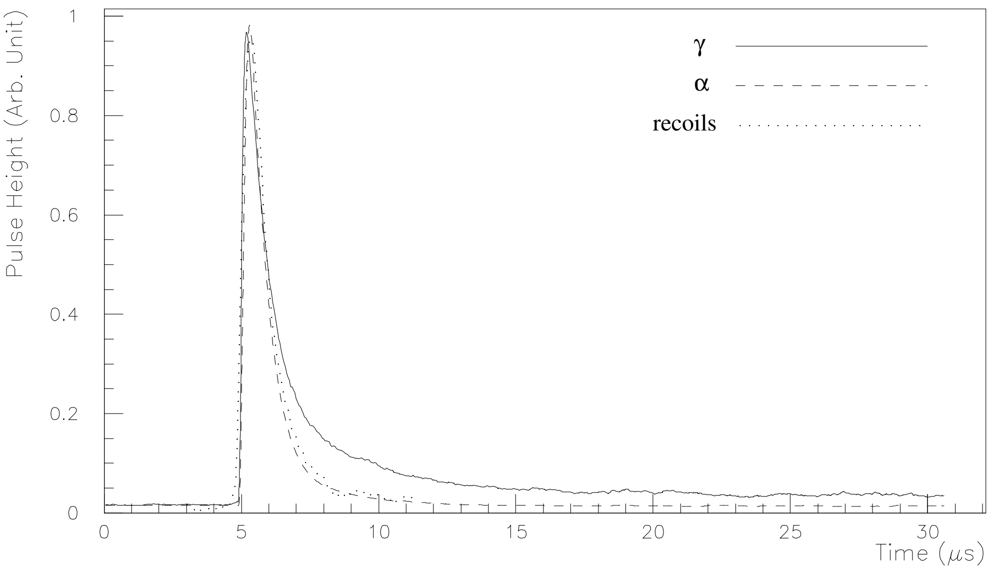

(b)

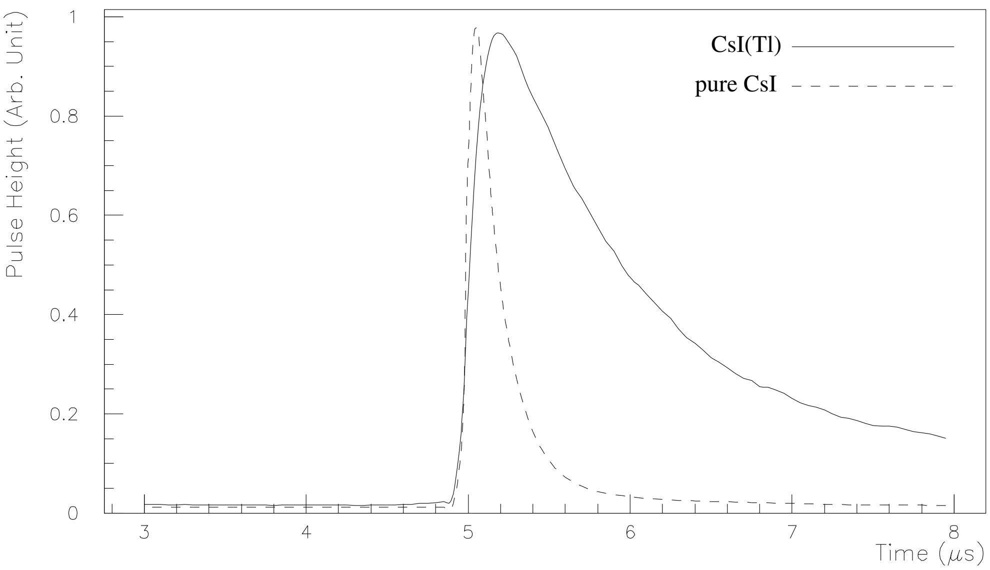

Figure 3: The average pulse shape for CsI(Tl) of (a) events due to γ-rays at 660 keV, α-particles at 5.4 MeV and nuclear recoils at 45 keV, and (b) its comparison with an undoped-CsI crystal, as recorded by the FADC module. The different decay times between γ's and the ions provide pulse shape discrimination capabilities.

(a)

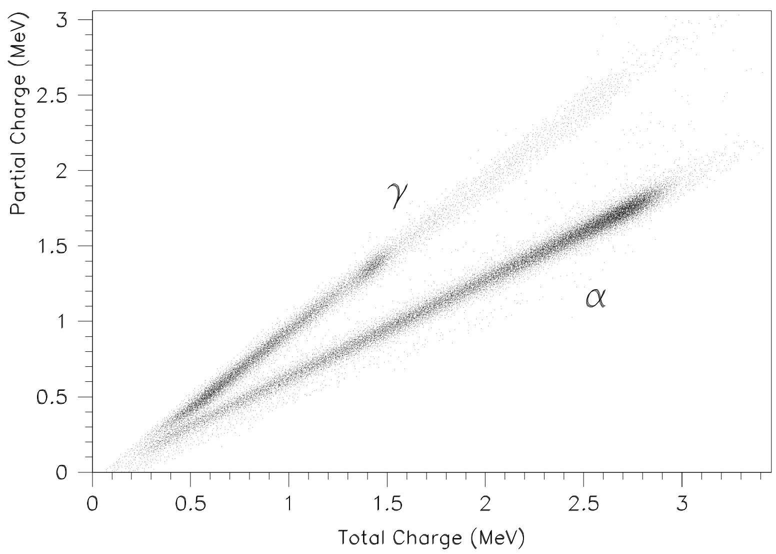

(b)

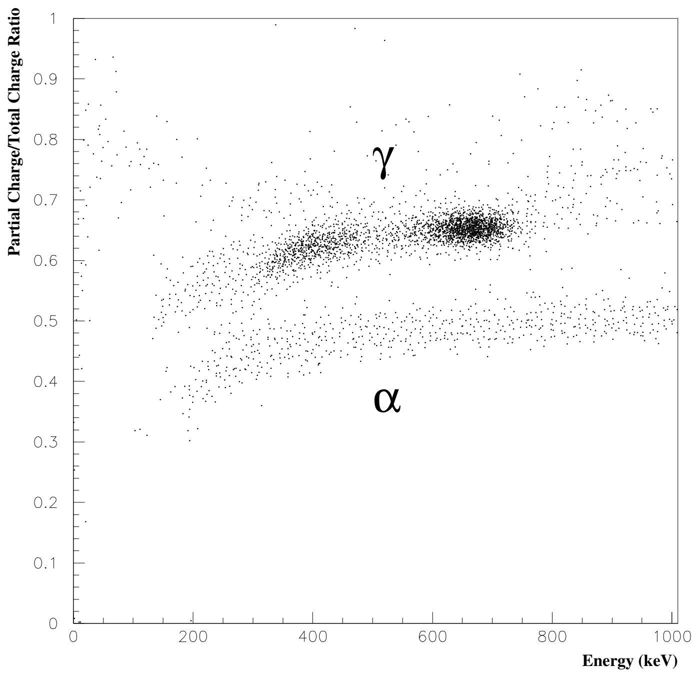

Figure 4: The partial charge versus total charge at (a) high and (b) low (<1 MeV) energy in a CsI(Tl) crystal, showing excellent (>99%) pulse shape discrimination capabilities to differentiate events due to α's and γ's. The α-events are from an ^{241}Am source placed on the surface of the crystal. The γ-events are due to ambient radioactivity in (a) and a ^{137}Cs source in (b).

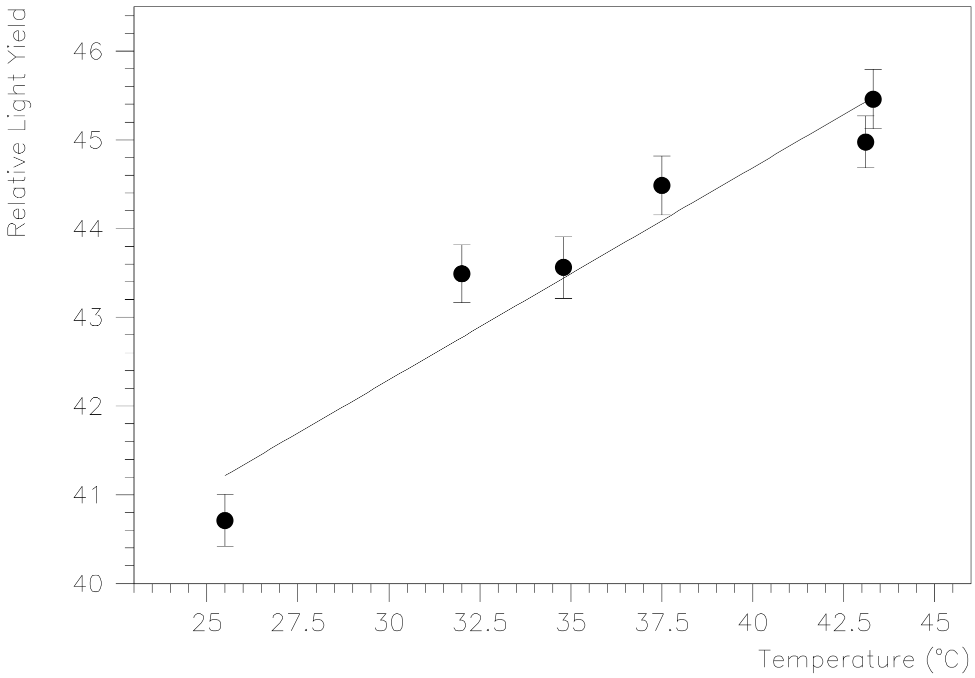

Figure 5: Measured temperature effects on the relative light yield of CsI(Tl) crystal viewed by a bi-alkaline photo-multiplier whose temperature coefficients have been corrected for.

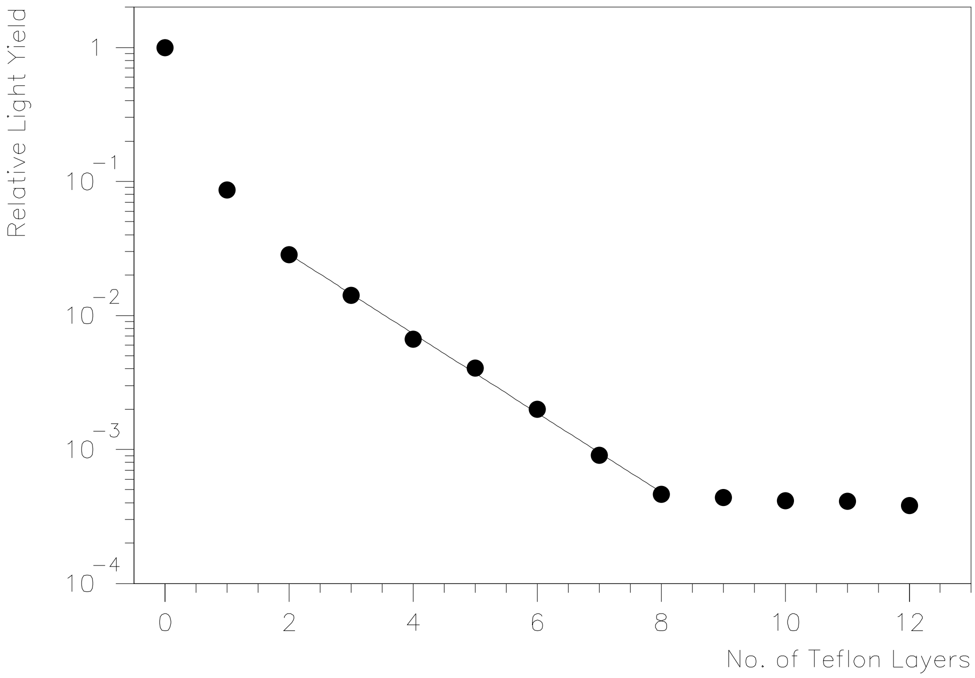

Figure 6: The measured pulse height of an LED signal after traversing a variable number of teflon sheets. Single photoelectron level is reached after 8 layers. Error bars are smaller than the symbols.

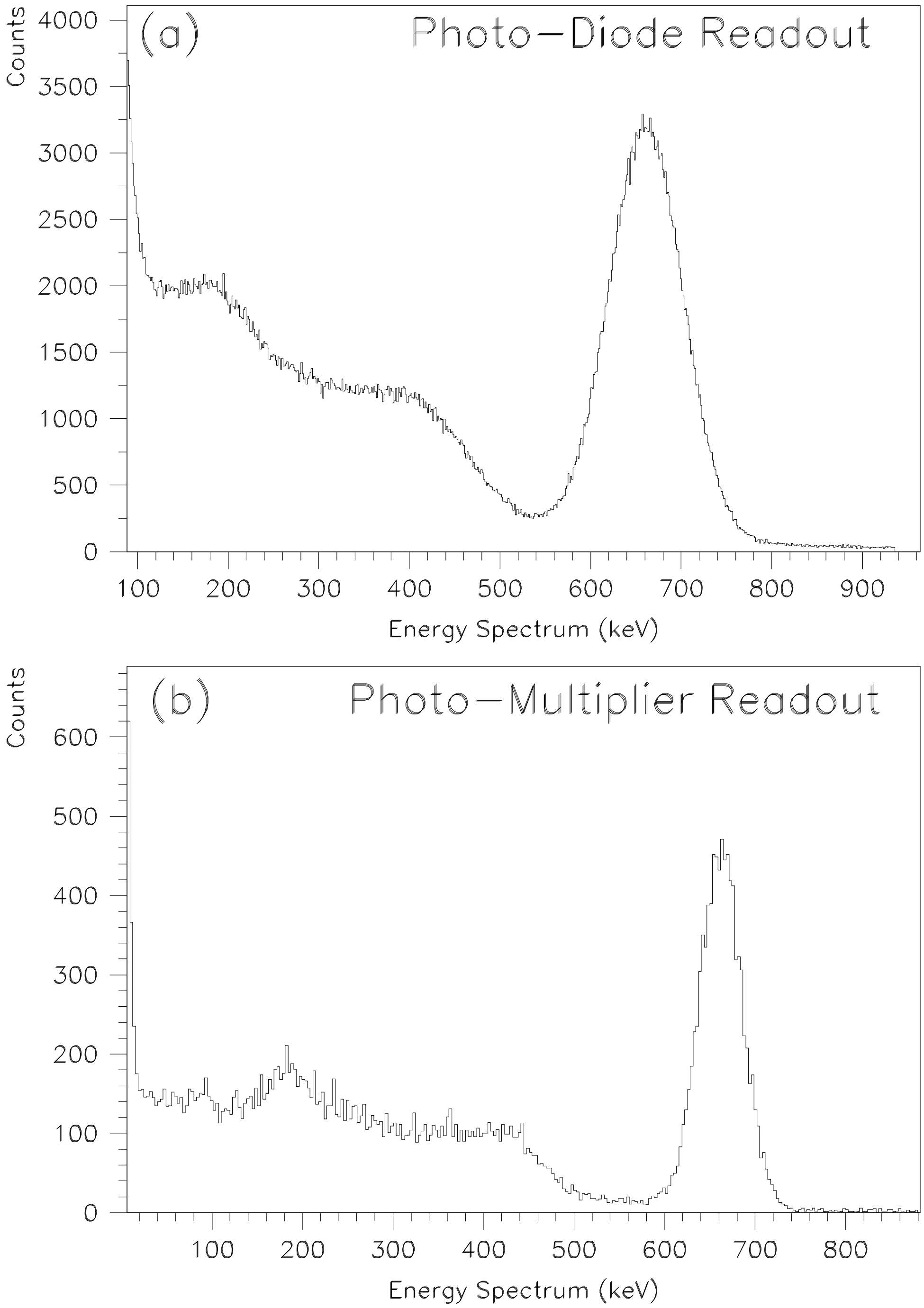

Figure 7: Comparison of measured energy spectra of ^{137}Cs on a CsI(Tl) crystal with 2.54 cm diameter and 2.54 cm length with (a) photo-diode and pre-amplifier and (b) photo-multiplier readout.

(a)

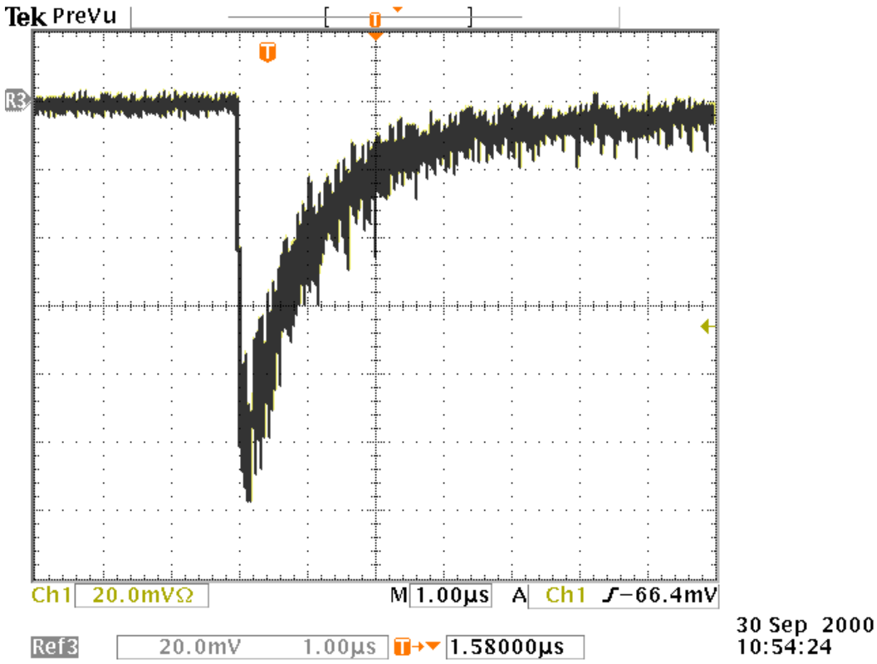

(b)

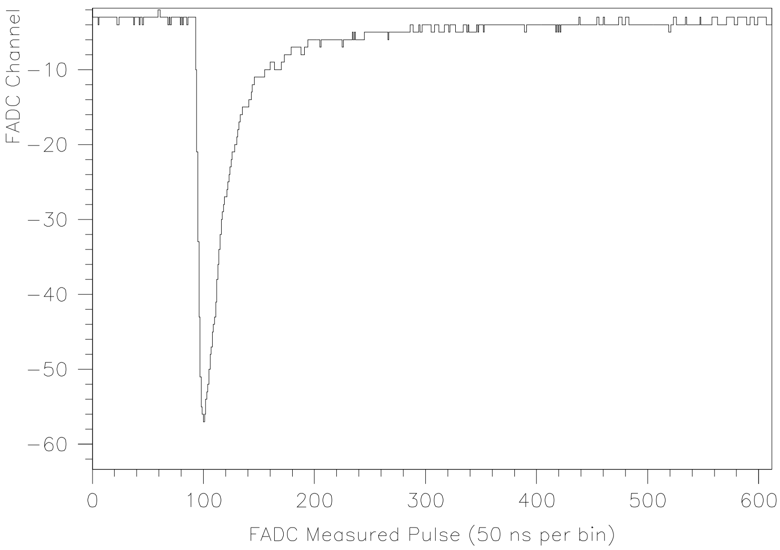

Figure 8: (a) Raw input signal from CsI(Tl)+PMT as recorded by a 100 MHz digital oscilloscope. Time axis: 1 μs per division. (b) Output signal after shaping from the Amplifier-Shaper as recorded by the FADC. Time axis: 5 μs per 100 FADC time bin.

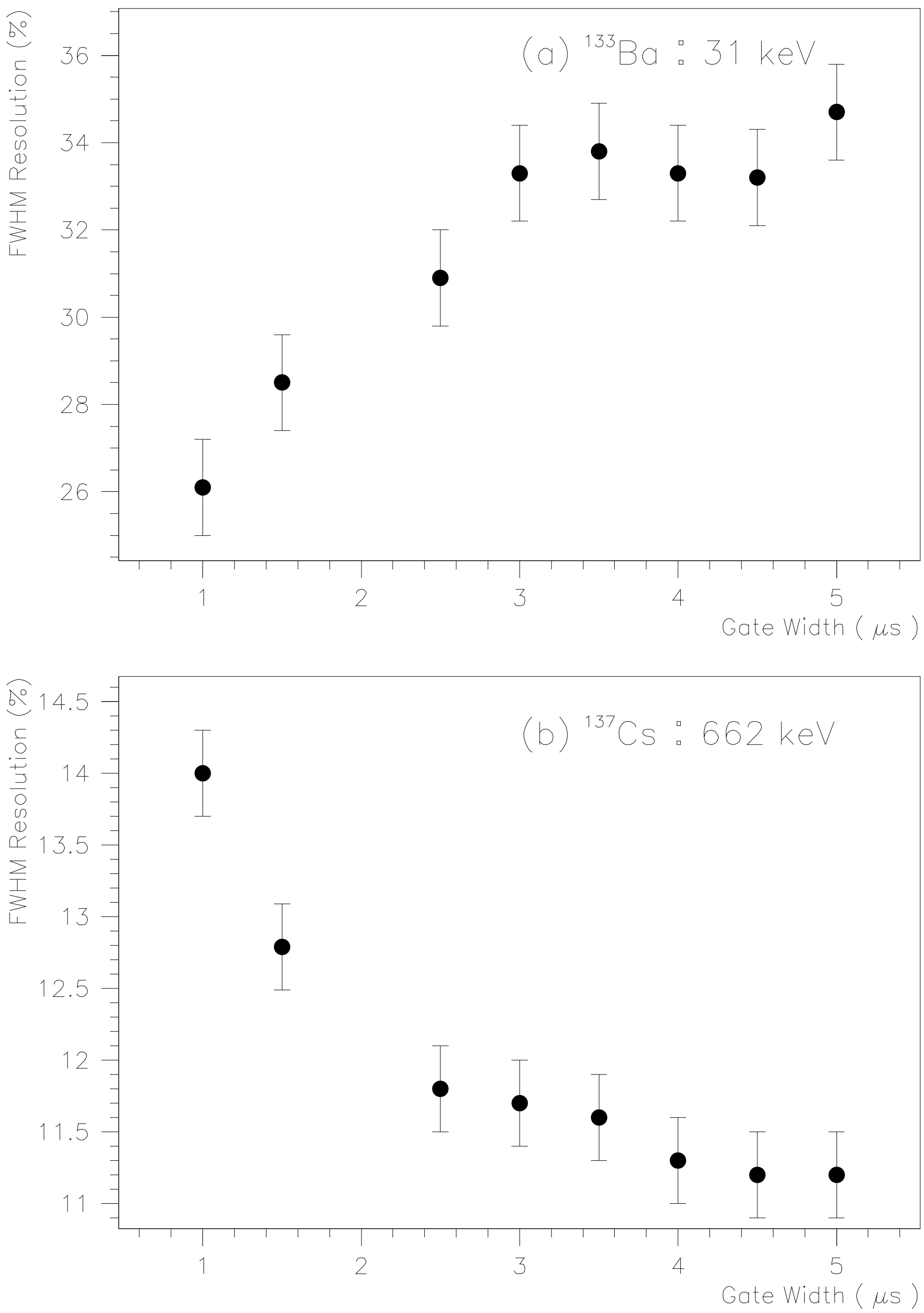

Figure 9: Measured FWHM energy resolution with different integration gate width for (a) E_γ=30 keV for ^{133}Ba, and (b) E_γ=662 keV for ^{137}Cs.

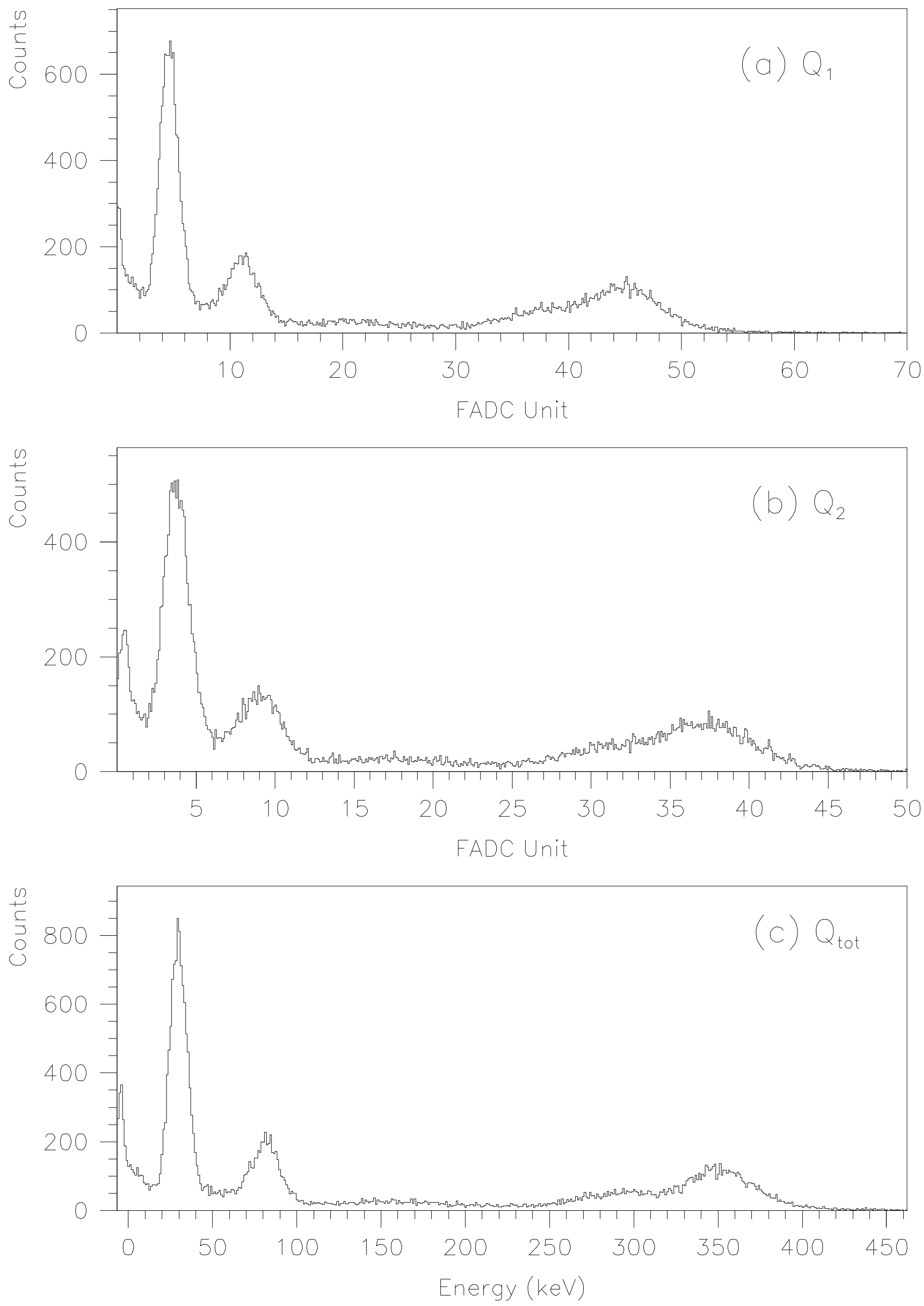

Figure 10: Measured spectra with a ^{133}Ba source for (a) Q_1, (b) Q_2 and (c) Q_{tot} with the L40/R crystal.

(a)

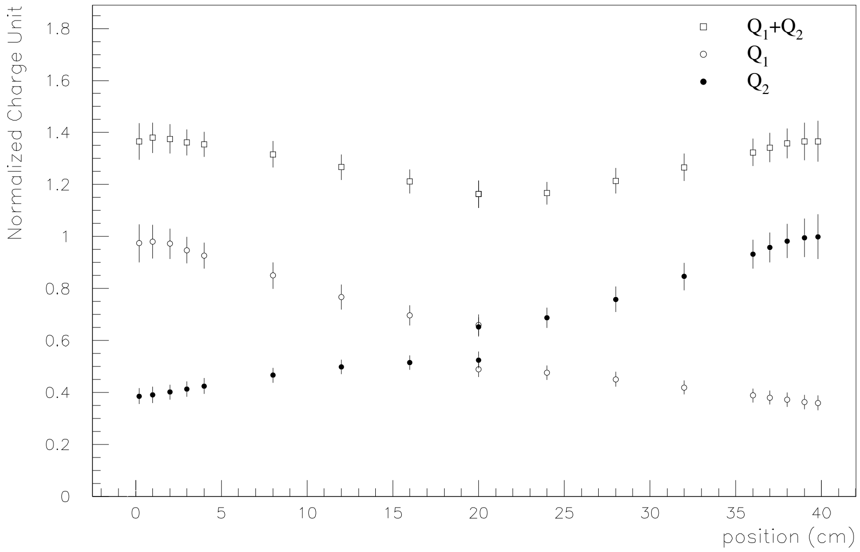

(b)

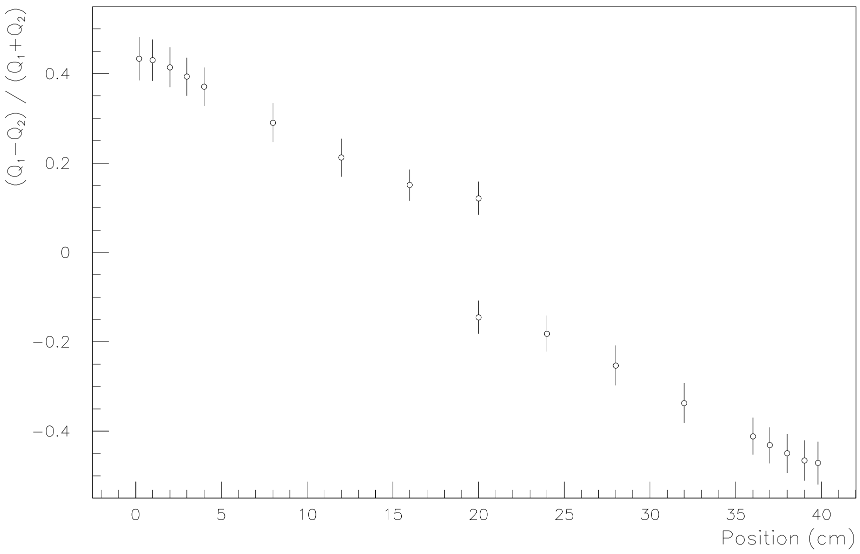

Figure 11: (a) Q_1, Q_2 and $Q_{tot} = Q_1 + Q_2$ and (b) $R = (Q_1 - Q_2)/(Q_1 + Q_2)$ along the longitudinal position of the L20+20/S crystal module. The charge unit is normalized to unity for both Q_1 and Q_2 at their respective ends. The error bars in (a) denote the width of the photo-peaks due to a ^{137}Cs source.

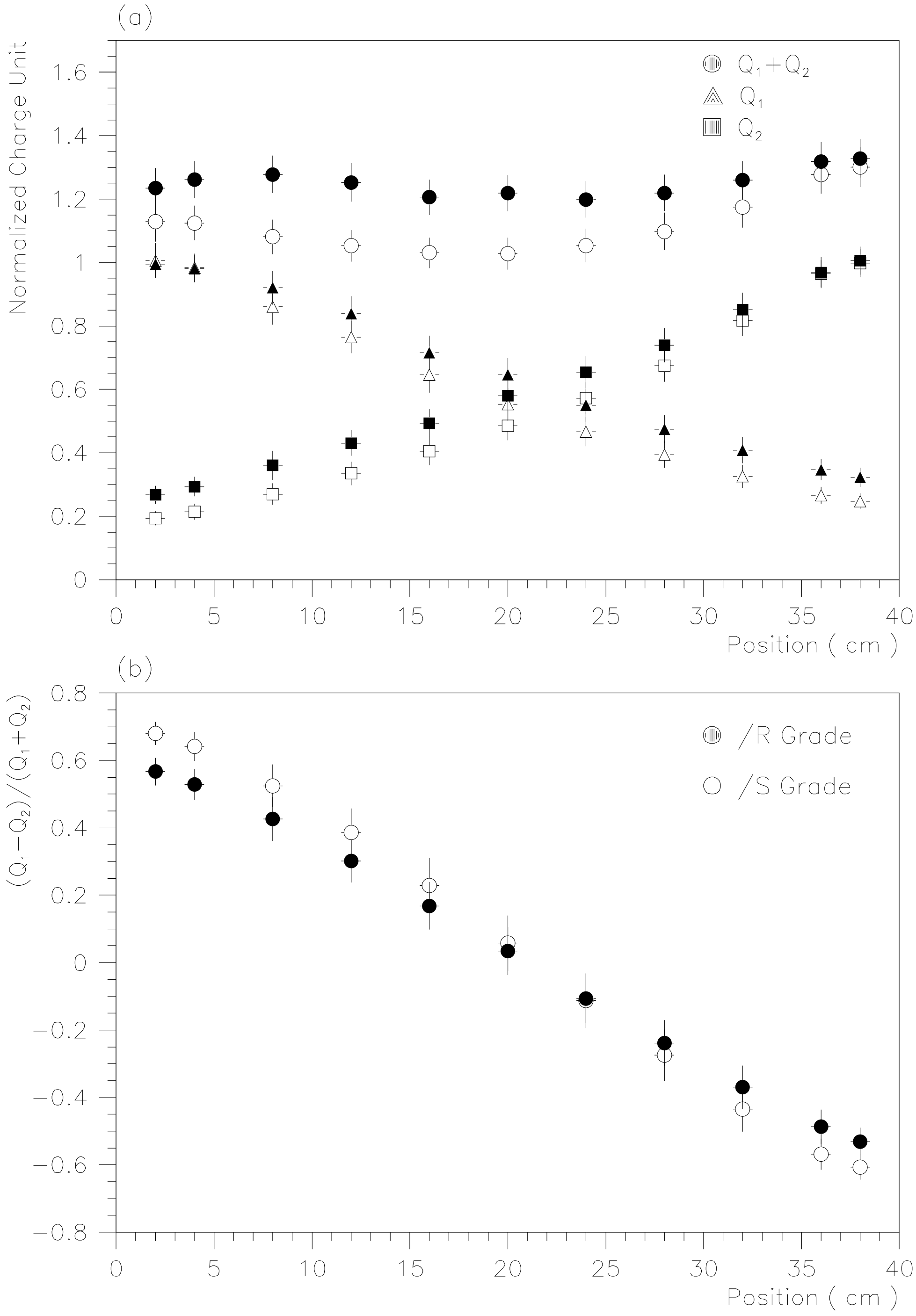

Figure 12: The measured variations of (a) Q_1, Q_2 and Q_{tot} and (b) the R-value along the longitudinal position of the L40/R and L40/S crystal module, denoted by shaded and open symbols, respectively.

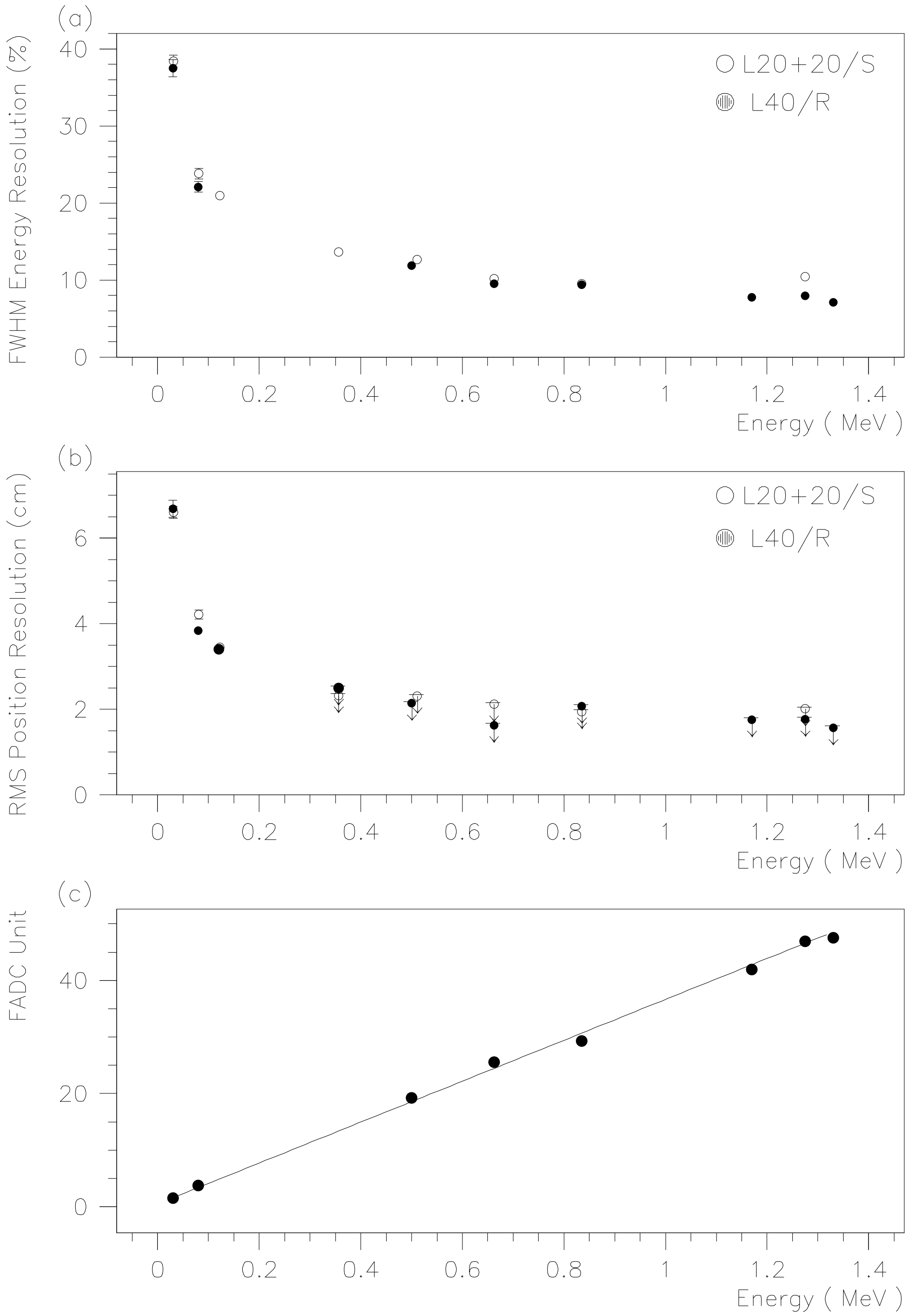

Figure 13: The variation of (a) FWHM energy resolution and (b) RMS position resolution with energy for L20+20/S and L40/R crystals, shown in open and closed symbols, respectively. Only upper limits are shown for the higher energy points in (b) since the events are not localized. (c) Illustration of the linearity of the energy response.

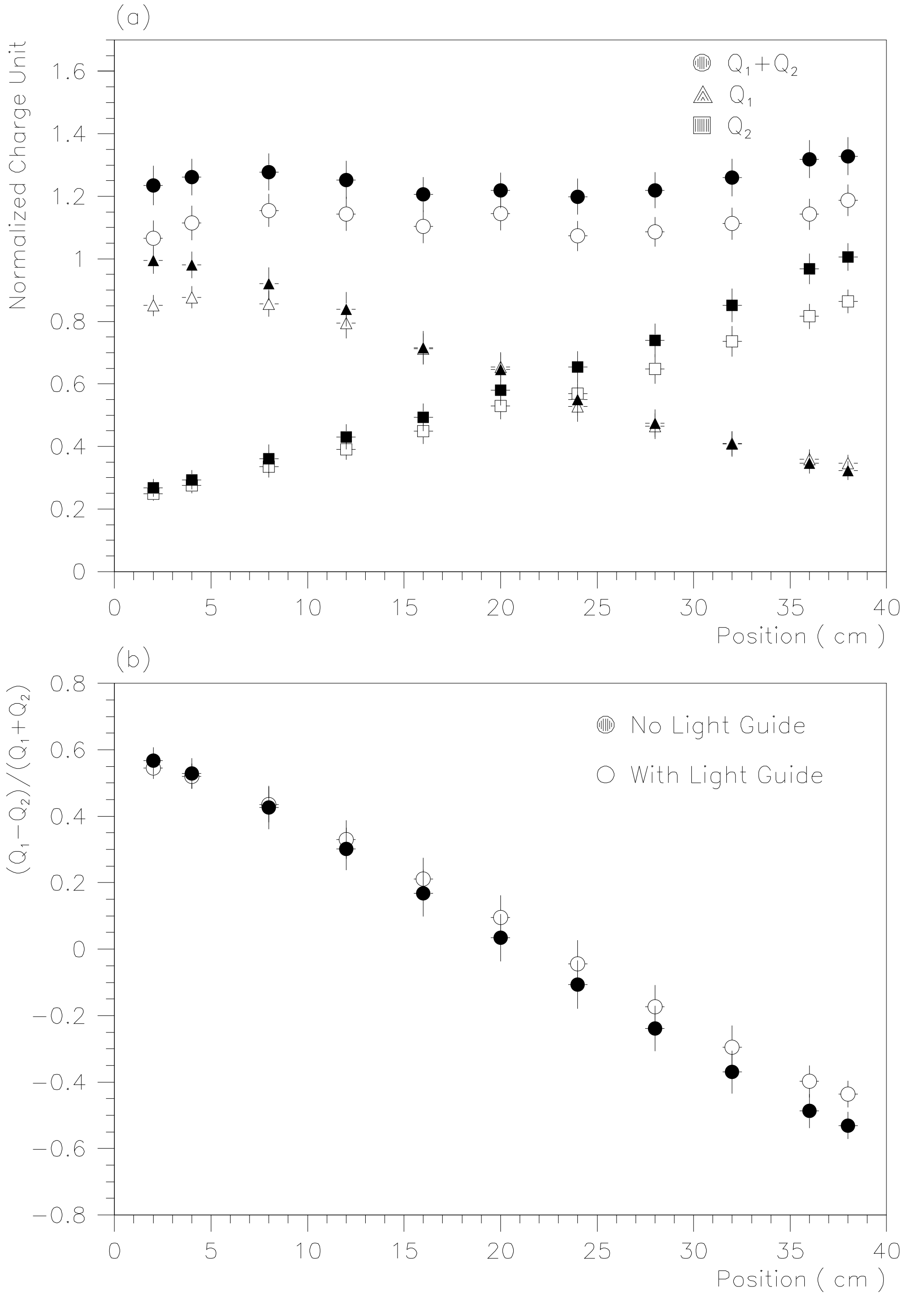

Figure 14: Comparisons of L40/R and L40/R+LG crystals, denoted by shaded and open symbols, respectively, for (a) Q_1, Q_2 and Q_{tot}, and (b) the R-values. The light guides are undoped-CsI with 3 cm in length at both ends.